The International Journal of Engineering and Science (IJES)
ISSN (e): 2319 – 1813 ISSN (p): 23-19 – 1805
|| Pages || PP 65-71 || 2020 ||

Numerical Study on the Effect of Leading Edge Tubercle on Symmetrical Airfoil at Low Reynolds Number

Jeena Joseph[1], A. Sathyabhama[2]
[1]*Department of Mechanical Engineering, National institute of Technology Karnataka, Surathkal, Karnataka, India*
[2]*Department of Mechanical Engineering, National institute of Technology Karnataka, Surathkal,Karnataka, India*

Corresponding Author:bhama72@gmail.com

----------ABSTRACT----------
The protrusions known as tubercle, on the leading edge of a humpback whale flipper help in the maneuverability of the whale despite its huge size. This work is computational study of stall characteristics and the flow pattern on a tubercledNACA 0021 airfoil and its comparison with a baseline airfoil at a low Reynolds number of 100 000. SST $k-\omega$ turbulence model based on unsteady RANS scheme is used to model the flow over airfoils at variosangles of attack. Lift and drag study concludes that airfoil with tubercles delays stall compared to baseline airfoil and has softer stall. Tubercled airfoil maintain high lift coefficients even at high angle of attack. From the flow pattern it is also seen that tubercled airfoil created a number of counter rotating vortices in the plane vertical to airfoil unlike the baseline airfoil. The relative strength of vortices on the suction and pressure surfaces of airfoil depends on the symmetricity of flow.
KEYWORDS: -*Tubercle, vortices, stall delay*

I. INTRODUCTION

The sinusoidal protruding on the leading edge of an airfoil capable of altering the fluid flow are called tubercles. The concept of tubercle is inspired from the protuberances seen on the flipper of a Humpback whale [1]. The cross of the flipper is similar to a NACA 63_4-21airfoil and tubercles on the flipper aids in keeping the flow attached to the surface for a wider range of angle of attack (AOA) and thereby delaying stall. It can be said that tubercles can function as a certain lift enhancement device which increases the maximum lift coefficient without much increase in drag [2].

Numerical study on NACA- 63_4-21 airfoil modified with tubercle showedlift enhancement as well as reduction in induced drag at a 10 degree angle of attack [3].Experimental study on NACA 0020 airfoil with tubercle showed a drastic increase in stall angle, reduction of drag in the post stall region and an increase in maximum coefficient of lift when compared to normal NACA 0021airfoil [4].However, an experimental study done by Stein and Murray [5]on a 2Dairfoil with sinusoidaledge of amplitude and wavelength comparable to that on the flipper on a humpback whale gave a contrary result. They found that the presence of tubercle increased drag and reduced lift when compared to airfoil with straight leading edge. Another study by Johari *et.al.* [6] also showed that tubercledairfoil degraded aerodynamic performance of the airfoil. A significant study by Murray et.al [7] concluded that sweeping of 3D airfoil can give improved aerodynamic characteristics.

Hansen [8] evaluated the aerodynamic characteristics of NACA 0021 and NACA 65-021 with varying amplitude and wavelength of the tubercle opined that reduction in tubercle amplitude leads to a hike C_{Lmax} and stall angle. However tubercles of larger amplitude performed better in the post stall regime. A reduction in wavelength leads enhancement of overall aerodynamic performance like maximum lift coefficient, stall angle, and post stall characteristics.

In this study, a comparison of the stall characteristic of tubercled NACA 0021 airfoil with a straight edge airfoil is made. The flow pattern of both airfoils are studied in an attempt to justify the variation in stall characteristics.

II. NUMERICAL ANALYSIS

Airfoil Model.

Two airfoils, one with straight leading edge and other with a sinusoidal leading edge are adopted for the study. The geometrical parameters of the airfoil are shown in Figure 1 and further enlisted in Table 1. The amplitude and wavelength for the tubercles airfoil is selected based on the experimental study done by Hansen *et.al* [8] giving best aerodynamic performance.

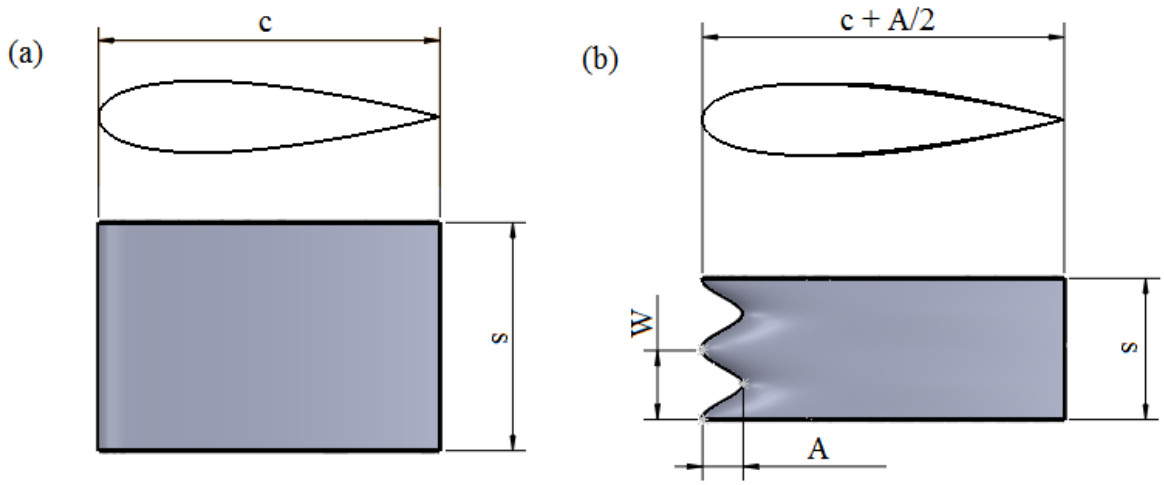

Figure 1:Schematic depicting the geometrical parameters for airfoils used in the study. a) Baseline airfoil b) tubercle airfoil

Label	Amplitude, A (mm)	Wavelength, W (mm)	Mean Chord, c (mm)	Span ,S (mm)
NACA 0021	N/A	N/A	150	100
NACA 0021 -T	9 (0.06 c)	31 (0.21 c)	150	62

Table 1 :Geometrical parameters of the modelled airfoils

Computational domain, grid and boundary conditions

A rectangular domain with structured and hexahedral elements is used as the domain of computation as shown in Figure 2.a. Domain is bounded by inlet at 10 chord lengths from the leading edge of airfoil, outlet at 15 chord lengths, far fields at 10 chord lengths on top and bottom. The lateral planes are designated as symmetry. The airfoil is given no slip wall condition.From a mesh sensitivity study, almost 13 lakh elements are used in the numerical analysis of tubercled airfoil. Due to the rather simpler geometry approximately same number of elements are used in normal airfoil also. Figure 2.b and 2.c shown the grid near normal airfoil and tubercle airfoil respectively. The boundary layer close to airfoil wall is resolved with large number of grids such that y^+=1 as per requirement of the turbulence model used.

Turbulence model

The turbulence model used is shear stress transport (SST) $k-\omega$, developed by Menter[9] which is a two equation eddy viscosity model -one for turbulent kinetic energy(k) and one for specific dissipation rate(ω).The transport equations for k and ω [10]are as given in equation 1 and 2:

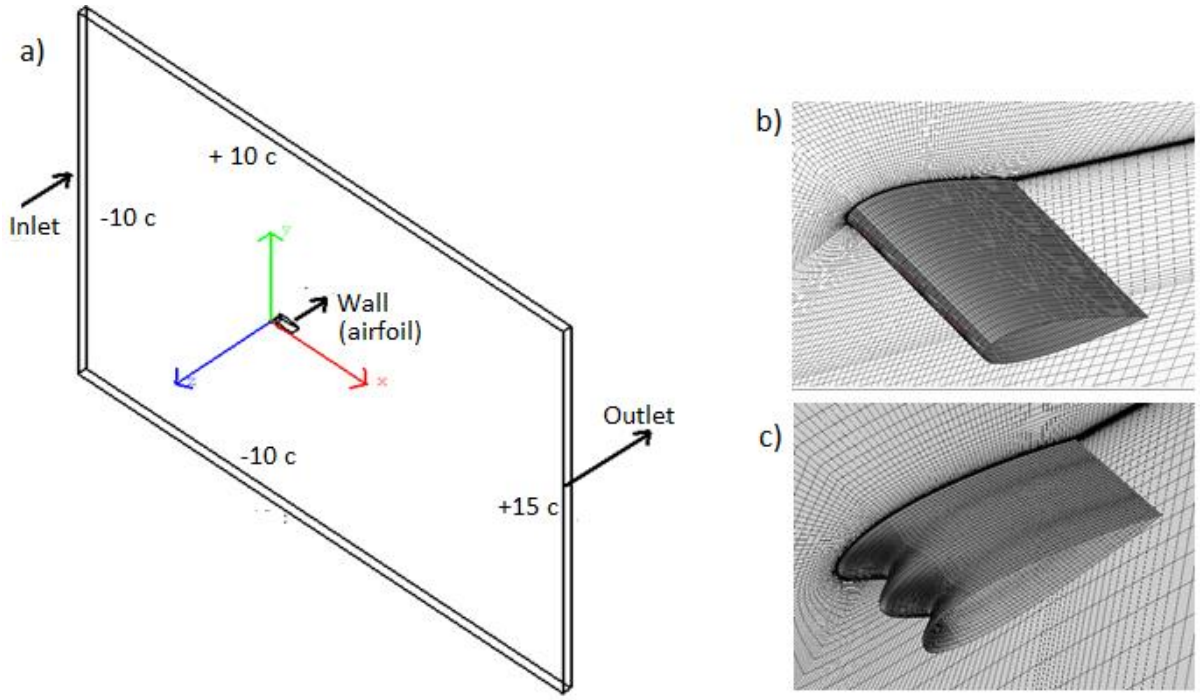

Figure 2: a) Computational domain and boundary conditions b) grid for baseline airfoil c) grid for tubercle airfoil

$$\frac{\partial}{\partial t}(\rho k) + \frac{\partial}{\partial x_i}(\rho k u_i) = \frac{\partial}{\partial x_j}\left(\Gamma_k \frac{\partial k}{\partial x_j}\right) + G_k - Y_k + S_k \quad (1)$$

$$\frac{\partial}{\partial t}(\rho \omega) + \frac{\partial}{\partial x_i}(\rho \omega u_i) = \frac{\partial}{\partial x_j}\left(\Gamma_\omega \frac{\partial \omega}{\partial x_j}\right) + G_\omega - Y_\omega + S_\omega + D_\omega \quad (2)$$

The term G_k in equation 1 denotes the turbulent kinetic energy production and is evaluated as $G_k = \mu_t S^2$ so as to be compatible with the Boussinesq hypothesis. Here S is the modulus of the mean rate of strain tensor given by $S \equiv \sqrt{2 S_{ij} S_{ij}}$.

The effective diffusivity of k if given by $\Gamma_k = \mu + \frac{\mu_t}{\sigma_k}$. μ_t denotes the turbulent viscosity and is given by $\mu_t = \frac{\rho k}{\omega} \frac{1}{max\left[\frac{1}{\alpha^*}, \frac{SF_2}{\alpha_1 \omega}\right]}$ and σ_k is the turbulent Prandtl number for k given by $\sigma_k = \frac{1}{\frac{F_1}{\sigma_{k,1}} + \frac{1-F_1}{\sigma_{k,2}}}$

Where,

$F_1 = \tanh(\Phi_1^4)$, $F_2 = \tanh(\Phi_2^4)$

$$\Phi_1 = min\left[max\left(\frac{\sqrt{k}}{0.09\omega y}, \frac{500\mu}{\rho y^2 \omega}\right), \frac{4\rho k}{\sigma_\omega D_\omega^+ y^2}\right]$$

$$D_\omega^+ = max\left[2\rho \frac{1}{\sigma_{\omega,2}} \frac{1}{\omega} \frac{\partial k}{\partial x_j} \frac{\partial \omega}{\partial x_j}, 10^{-10}\right]$$

$$\Phi_2 = \left[max\left(2\frac{\sqrt{k}}{0.09\omega y}, \frac{500\mu}{\rho y^2 \omega}\right)\right]$$

In the equation 1, term Y_k denotes the turbulent kinetic energy dissipation and is evaluated as $Y_k = \rho \beta^* k \omega$

Where

$\beta^* = \beta_i^*[1 + \zeta^* F(M_t)]$,

$$\beta_i^* = \beta_\infty^* \left(\frac{\frac{4}{5} + \left(Re_t/R_\beta\right)^4}{1 + \left(Re_t/R_\beta\right)^4}\right)$$

$\zeta^* = 1.5$, $\beta_\infty^* = 0.09$, $R_\beta = 8$.

The compressibility function $F(M_t) = \begin{Bmatrix} 0 & M_t \le M_{t0} \\ {M_t}^2 \le {M_{t0}}^2 & M_t > M_{t0} \end{Bmatrix}$

Where, ${M_t}^2 \equiv \frac{2k}{a^2}$, $M_{t0} = 0.25$,$a = \sqrt{\gamma RT}$

Similarly the term G_ω in equation 2 denotes the ω generation and is evaluated as $G_\omega = \frac{\alpha}{v_t} G_k$.The coefficient α is given by $\alpha = \frac{\alpha_\infty}{\alpha^*}\left(\frac{\alpha_0 + Re_t/R_\omega}{1+Re_t/R_\omega}\right)$

$\alpha_\infty = F_1\alpha_{\infty,1} + (1-F_1)\alpha_{\infty,2}$, where,$\alpha_{\infty,1} = \frac{\beta_{i,1}}{\beta^*_\infty} - \frac{\kappa^2}{\sigma_{w,1}\sqrt{\beta^*_\infty}}$ and $\alpha_{\infty,2} = \frac{\beta_{i,2}}{\beta^*_\infty} - \frac{\kappa^2}{\sigma_{w,2}\sqrt{\beta^*_\infty}}$

$R_\omega = 2.95, Re_t = \frac{\rho k}{\mu\omega}$, $\alpha^* = {\alpha_\infty}^*\left(\frac{{\alpha_0}^* + Re_t/R_k}{1+Re_t/R_k}\right)$, $R_k = 6$, ${\alpha_0}^* = 0.024$, $\kappa = 0.41$

The effective diffusivity of ω is given by$\Gamma_\omega = \mu + \frac{\mu_t}{\sigma_\omega}$. σ_ω is the turbulent Pandtl number for ω given by $\sigma_\omega = \frac{1}{\frac{F_1}{\sigma_{\omega,1}} + \frac{1-F_1}{\sigma_{\omega,2}}}$.

In equation 2,Y_ω denotes the dissipation of ω and is given by $Y_k = \rho\beta\omega^2$

Where $\beta = \beta_i\left[1 - \frac{\beta^*_i}{\beta_i}\zeta^* F(M_t)\right]$ and $\beta_i = F_1\beta_{i,1} + (1-F_1)\beta_{i,2}$

It is known that SST k omega is a blend of k epsilon and k omega. Thus transformation of k-epsilon model to equations based on k and omega introduces a term D_ω as seen in equation 2 which is defined as $D_\omega = 2(1-F_1)\rho\frac{1}{\omega\sigma_{\omega,2}}\frac{\partial k}{\partial x_j}\frac{\partial \omega}{\partial x_j}$

The various constants used in SST models are:-

$\sigma_{k,1} = 1.176$, $\sigma_{k,2} = 1$,$\sigma_{\omega,1} = 2$, $\sigma_{\omega,2} = 1.168$, $a_1 = 0.31$, $\beta_{i,1} = 0.075$, $\beta_{i,2} = 0.0828$, $\alpha^*_\infty = 1$, $\alpha_\infty = 0.52$,$\alpha_0 = 1/9$, $\beta^*_\infty = 0/09$.

Numerical scheme validation

The solver and the boundary conditions are validated by comparimg the value of lift coeffient and drag cooefficient obtained from simulation with experimental values presented by Shedahl and Klimas[11].Fiure 3.a depicts the lift coefficient with varying AOA respectively.There is an average varation of 11 % for lift coefficient when compared to experimental results . Figure 3.b depicts the drag coefficient and a 13 % variation is seen in the prestall region. It is also obseved that the the coeffient of drag is under predicted in the post stall region which could be the incapability of solver to predict pressure drag caused by flow separation.However, it is seen that there good agreement of the numerical value with the experimental one.The difference in lift and drag between the experimental and numerical results could be due to limitation of RANS model used compared to complex models LES or DNS.

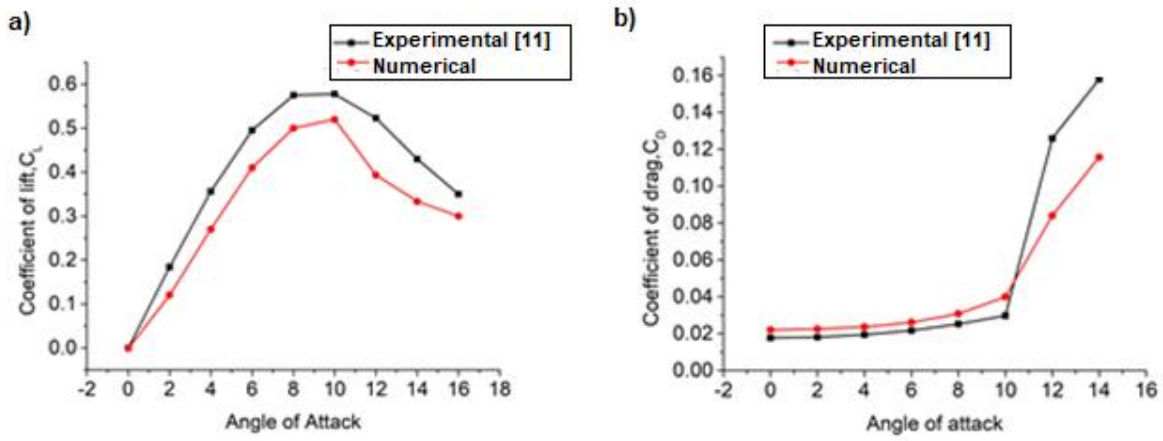

Figure 3: Comparison of numerical and experimental results of NACA 0021 [11] a) Lift characteristics b) Drag characteristics

III. RESULT VIEW

Lift and Drag

Figure 4.a shows a comparison of lift coefficient at various angle of attacks for a normal unmodified airfoil and a tubercle airfoil. It is seen that the normal airfoil stalls at an angle of attack 10 degree. Beyond 10 degree the lift is decreased drastically showing a steep stall characteristic. However for a tubercled airfoil even after 10 degrees, lift is not degraded drastically and there is a soft stall. In the drag characteristics shown in Figure 4.b it is seen that tubercle has no effect at very small angle of attack (0 and 2 degree) but in the pre stall region increases drag. Similar results were obtained in the experimental study done by Watts and Fish [3].It can be said that the tubercled airfoil has superior aerodynamic characteristics in the post stall region compared to normal airfoil.

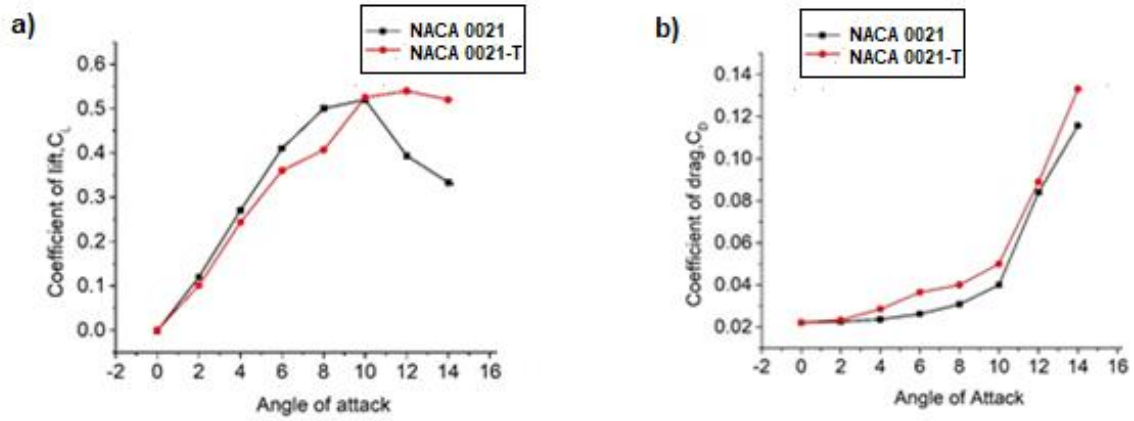

Figure 4: Comparison of normal and tubercle NACA 0021 airfoil a) Lift characteristics b)Drag characteristics

Velocity Streamlines

Figure 5 shows a comparison of streamlines for both airfoils at 0 dgree AOA. As seen in Figure 5.a the flow pass over the airfoil smoothly and leave the trailing edge.However for the tubercled airfoil near the trailing edge the flow is convected around some arbitary point which forms 3D vortices which are counter rotating as seen in Figure 5.b and will be discused further in section 3.3

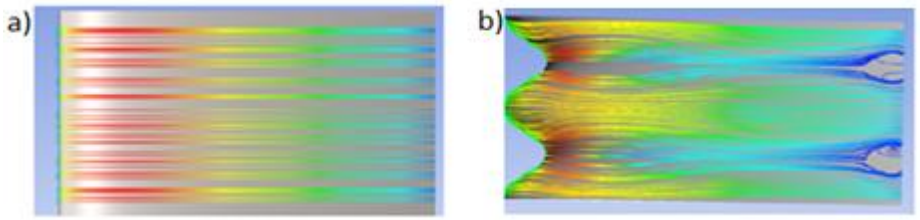

Figure 5: Streamlines on suction surface a) normal airfoil b) tubercle airfoil

The changes that occur in streamlines over tubercle airfoil with varying angle of attack is depicted in Figure 6.It is seen that as the the angle of attack increases the flow convection starts early.This phenomenon is unlikely to happen for a normal airfoil,where as angle of attack increased, flow separates and leave the surface but do not produce counter rotating vortices.

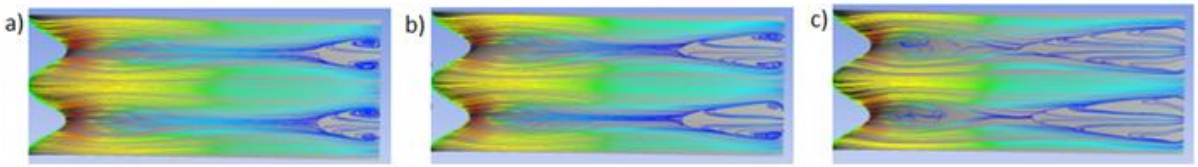

Figure 6: Streamlines on tubercle airfoil a) 2^0 AOA b) 4^0 AOA c) 6^0 AOA

Streamwise vorticity

To study the contours of streamwise vorticity and turbulent kinetic energy of at the wake region, four planes namely A, B, C and D are chosen at distance 30 mm, 90 mm, 150 mm and 250 mm away from the airfoil trailing edge as shown in Figure 7. Figure 8, 9 and 10 shows the contours of streamwise vorticity at these planes for AOA 0^0, 4^0, and 6^0.

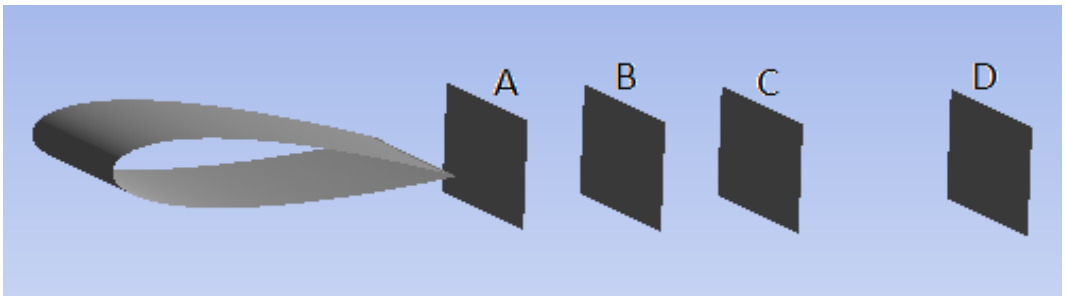

Figure 7: Diagram showing location of planes used for visualization

As seen in Figure 8, when the AOA is zero there pairs of counter rotating vortices of equal strength are seen on top and bottom side of the airfoil (red colour indicate positive values and therefore clockwise vortex and blue indicate counter clockwise vortex).As we move away in the wake region the vortices are still prominent though it diffused into a larger area. It is also seen that the maximum magnitude of vorticity core decreases as moving further away in the wake region. The symmetric nature of vortex can be attributed to the symmetrical flow around the airfoil section, NACA 0021 being a symmetrical airfoil.

However as AOA increases the strength of vortices on the top goes on increasing while it decreases on the bottom side as seen in Figure 9 and Figure 10. As the angle of attack reaches 6 degrees (Figure 10) the vortices on the bottom side are barely seen.

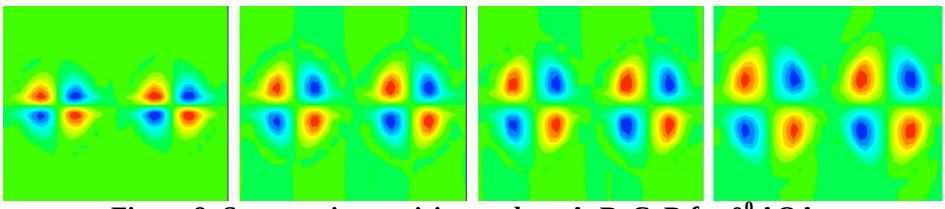

Figure 8: Stream wise vorticity at plane A, B, C, D for 0^0 AOA

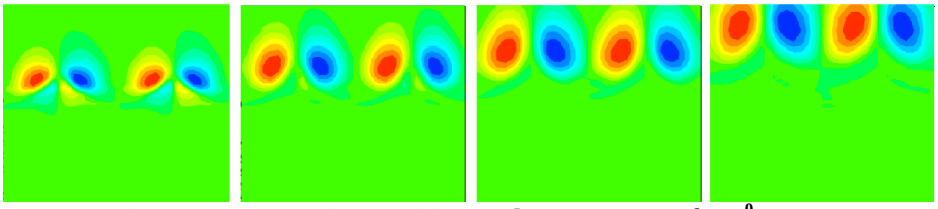

Figure 9: Stream wise vorticity at plane A, B, C, D for 2^0 AOA

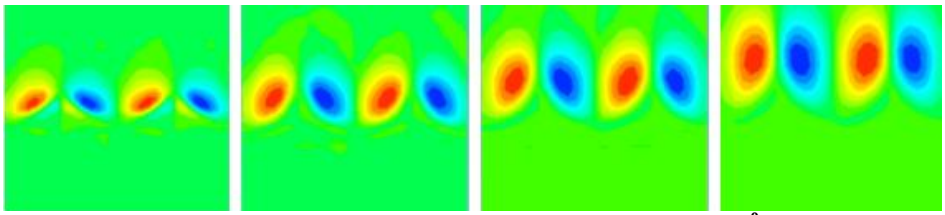

Figure 10: Stream wise vorticity at plane A, B, C, D for 4^0 AOA

Turbulent kinetic energy (TKE)

Figure 11.a and 11.b shows the turbulent kinetic energy contours at plane A for normal and tubercle airfoil respectively. It is seen that TKE is distributed uniformly for normal airfoil whereas for tubercle airfoil it is larger in the trough region. When moving further downstream to plane B the TKE dissipates over larger area as seen in Figure 11.c and 11.d.

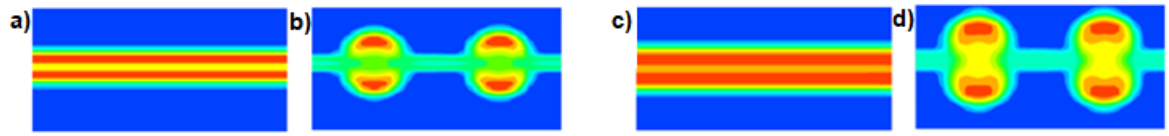

Figure 11: TKE contours a) normal airfoil-plane A b) tubercle airfoil-plane A c) normal airfoil-plane B d) tubercle airfoil-plane B

The variation of TKE with change in AOA is shown in Figure 12.Onset of turbulence happen in trough for all airfoils. As the AOA increases from 0 to 6 the turbulence in the flow starts to develop earlier.

.

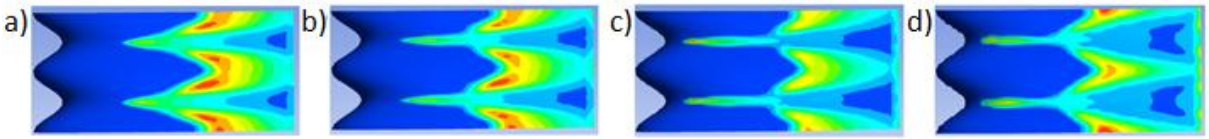

Figure 12: TKE on surface of tubercle airfoil a) AOA 0^0 b)AOA 2^0 c)AOA 4^0 d) AOA 6^0

IV. CONCLUSION

A simple modification on the leading edge of an airfoil drastically alters the flow patter and aerodynamic characteristics. A sinusoidal leading edge on airfoil is seen to have improved the post stall characteristics of NACA 0021 airfoil. The leading edge tubercle creates counter rotating vortices in the trough region which aid in altering the flow pattern. These counter rotating vortices could reenergize the boundary layer and keep the flow attached to the airfoil surface even at high angle of attack. It can be concluded that the vortices created by the tubercles cause for the delayed stall and better aerodynamic performance in the post stall region.

REFERENCE

[1]. Benke, H. (1993). Investigations on the osteology and the functional morphology of the flipper of whales and dolphins (Cetacea). Invest. Cetacea 24, 9-252

[2]. Fish, F.E. and Battle, J.M., Hydrodynamic design of the humpback whale flipper, J. Morp., 225:51-60, 1995.

[3]. Watts, P. and Fish, F.E., The Influence of Passive, Leading Edge Tubercles on Wing Performance, Proc. Of Unmanned Untethered Submersible Technology (UUST), Durham, NH, August, 2001

[4]. D.S. Miklosovic, M.M. Murray, L.E. Howle, and F.E. Fish: "Leading-edge Tubercles Delay Stall on Humpback Whale (Megapteranovaeangliae) Flippers". Physics of Fluids, Vol. 16, No. 5 (2004).

[5]. Stein, B. & Murray, M.M., Stall mechanism analysis of humpback whale flipper models, Proc. of Unmanned Untethered Submersible Technology (UUST), Durham, NH, August 2005

[6]. Johari, H., Henoch, C., Custodio, D., Levshin, A.: Effects of leading edge protuberances on airfoil performance. AIAA J. 45(11), 2634–2642 (2007) Kristy L.

[7]. Murray, M.M., Miklosovic D.S., Fish, F.E., Howle, L.E., Effects of leading edge tubercles on a representative whale flipper model at various sweep angles, Proc.of Unmanned Untethered Submersible Technology (UUST),Durham, NH, August 2005

[8]. Hansen, Richard M. Kelso, and Bassam B. Dally: "Performance Variations of Leading-Edge Tubercles for Distinct Airfoil Profiles", AIAA Journal, Vol. 49, No. 1 (2011)

[9]. Menter, F. R. (1993), "Zonal Two Equation k-ω Turbulence Models for Aerodynamic Flows", AIAA Paper 93-2906

[10]. Ansys fluent theory guide.Fluent - ANSYS Inc., USA, 2011

[11]. Sheldahl, R. E., Klimas, P. C., 1981. Aerodynamic characteristics of seven symmetrical airfoil sections through 180-degree angle of attack for use in aerodynamic analysis of vertical axis wind turbines. Sandia National Laboratories